Dalton Transactions

Accepted Manuscript

ROYAL SOCIETY OF CHEMISTRY

www.rsc.org/dalton

Dalton Transactions

RSCPublishing

ARTICLE

A novel greenish yellow-orange red $Ba_3Y_4O_9:Bi^{3+},Eu^{3+}$ phosphor with efficient energy transfer for UV-LEDs

Cite this: DOI: 10.1039/x0xx00000x

Kai Li,[ab] Hongzhou Lian,*[a] Mengmeng Shang[a] and Jun Lin*[a]

Received,
Accepted

DOI: 10.1039/x0xx00000x

www.rsc.org/

A series of novel color-tunable $Ba_3Y_4O_9:Bi^{3+},Eu^{3+}$ phosphors were first prepared via the high-temperature solid-state reaction route. The effect of Bi^{3+} concentration on the emission intensity of $Ba_3Y_4O_9:Bi^{3+}$ is investigated. The emission spectra of the $Ba_3Y_4O_9:Bi^{3+},Eu^{3+}$ phosphors present both a greenish yellow band centered at 523 nm of Bi^{3+} and many characteristic emission lines of Eu^{3+}, deriving from the allowed $^3P_1$-$^1S_0$ transition of the Bi^{3+} ion and the $^5D_0$-^7F_J transition of the Eu^{3+} ion, respectively. The energy transfer phenomenon from Bi^{3+} to Eu^{3+} ions is observed under UV excitation in Bi^{3+}, Eu^{3+} co-doped $Ba_3Y_4O_9$ phosphors, and their transfer mechanism is demonstrated to be a resonant type via dipole-quadrupole interaction. The critical distance between Bi^{3+} and Eu^{3+} of energy transfer effect was calculated via the concentration quenching and spectral overlap methods. Results show that color tuning from greenish yellow to orange red can be realized by adjusting the mole ratio of Bi^{3+} and Eu^{3+} concentrations based on the principle of energy transfer. Moreover, temperature-dependence PL properties, CIE chromaticity coordinates and quantum yields of $Ba_3Y_4O_9:Bi^{3+},Eu^{3+}$ phosphors were also supplied. It illustrates that as-prepared $Ba_3Y_4O_9:Bi^{3+},Eu^{3+}$ phosphors can be as potential candidates for color-tunable phosphors applied in UV-pumped LEDs.

1. Introduction

Recently, considerable attention has been focused on the development of white lighting-emitting diodes (w-LEDs), which is considered to be the next generation of lighting source replacing the conventional incandescent and fluorescent lamps owing to its superior merits such as high luminous efficiency, energy saving, long operation lifetime and environmentally friendliness.[1] As an important section in LEDs, the phosphor also attracts extensive attention, therefore, many investigations have been devoted into the development of new phosphors. Currently, Commercial w-LEDs is fabricated via the combination of a GaN blue-emitting LED chip and YAG:Ce^{3+} yellow phosphor. However, the deficiency of red component in it results in a poor color-rendering index (CRI) and high correlated color temperature (CCT), which limits its use in more vivid applications.[2] In order to overcome these issues, another method involving the employment of UV LED chips with tricolor (blue, green and red) is adopted. Therefore, searching for novel phosphors with different emission colors is high needed. Among these, red-emitting phosphors are more desired to be obtained.

It is well known that the absorption bands of Bi^{3+} are usually attributed to the allowed $^1S_0$-$^1P_1$ and $^1S_0$-$^3P_1$ transitions.[3] It can not only as a solo activator emitting the blue to green even red band with the wavelength of 400-700 nm attributed to its 6s6p→$6s^2$ transition upon UV excitation in an appropriate crystal field originating from covalence, coordination number and site symmetry, but also usually acts as a sensitizer to enhance Eu^{3+} emission in a large amount of hosts such as fluorophosphates, germinates, aluminates, silicates, rare earth oxides, molybdates, tungstates and vanadates.[4] Eu^{3+} is a preferable choice as an activator ion with red emission via $^5D_0$-$^7F_2$ transition at about 613 nm, which has been used in most commercial red phosphors.[5] In addition, the nature of this transition strongly depends on its local environment and can be utilized to probe the site symmetry in the host. Many excitation lines with the wavelength range of 300-500 nm are derived from the intra-configurational 4f-4f transition of dopant Eu^{3+}. However, rare reports have been devoted into Bi^{3+} and Eu^{3+} co-doped oxide phosphors excluding rare earth oxide although oxide phosphors have recently obtained a lot of attention for applications such as display devices and lighting attributed to their higher chemical stability relative to sulfide phosphors. As far as we know, the Bi^{3+} and Eu^{3+} doped $Ba_3Y_4O_9$ phosphors have not ever been reported. Herein, the phases, morphologies, and optical properties of the $Ba_3Y_4O_9:Bi^{3+},Eu^{3+}$ phosphors thus produced were then first synthesized and investigated. Moreover, the energy transfer properties from Bi^{3+} to Eu^{3+} ions also have been studied in detail. As a result, eye-visible emissions with tunable color from greenish yellow to orange red are easily generated by simply adjusting Eu^{3+} content in $Ba_3Y_4O_9:Bi^{3+},Eu^{3+}$ phosphors based on the energy transfer from Bi^{3+} to Eu^{3+} ions under UV excitation.

2. Experiment section

2.1 Materials and preparation

[a]*State Key Laboratory of Rare Earth Resource Utilization, Changchun Institute of Applied Chemistry, Chinese Academy of Sciences, Changchun 130022 (P. R., China.). Email: jlin@ciac.ac.cn; Fax: +86-431-85698041; Tel: +86-431-85262031*
[b]*University of Chinese Academy of Sciences, Beijing 100049 (P. R., China.)*

A variety of objective powder phosphors with the nominal composition of $Ba_3Y_{4-x-y}O_9:xBi^{3+},yEu^{3+}$ (abbreviated as BYO:xBi^{3+},yEu^{3+}, x = 0-0.24, y = 0-0.32) were prepared via the conventional high-temperature solid-state reaction method. The raw materials $BaCO_3$ (A.R.), Bi_2O_3 (99%), Y_2O_3 (99.99%) and Eu_2O_3 (99.99%), without any purity, were first weighed under the stoichiometric ratio. After 15 min grinding and mixing with addition of appropriate alcohol, the mixture was dried in the oven with the stationary temperature of 60 ℃, then they were reground for 1 min, placed into the crucible and transformed to the tube furnace to sinter at 1400 °C for 5 h to gain the final samples under air atmosphere condition. After calcination, the samples were furnace-cooled to room temperature and crushed into powders for the next characterization.

2.2 Characterization

All measurements were carried on utilizing the finely ground powder. D8 Focus diffractometer was used to identify the phase purity of samples with the scanning rate of 10°min^{-1} in the 2θ range from 10° to 65° with graphite-monochromatized Cu K_α radiation (λ = 0.15405 nm). The morphology of the sample was observed using a scanning electron microscope (SEM, S-4800, Hitachi). The Hitachi F-7000 spectrophotometer equipped with a 150 W xenon lamp as the excitation source was used to do the photoluminescence (PL) measurements. The luminescence decay lifetimes were measured and obtained from a Lecroy Wave Runner 6100 Digital Osilloscope (1 GHz) using a tunable laser (pulse width = 4 ns, gate = 50 ns) as the excitation (Contimuum Sunlite OPO) source. PL quantum yields (QYs) of phosphors were obtained directly by the absolute PL quantum yield measurement system (C9920−02, Hamamatsu Photonics K. K., Japan). All the above measurements were performed at room temperature (RT). Additionally, the temperature-dependent (298-473 K) PL spectra were measured on Edinburgh Instruments FLSP-920 with a temperature controller.

3. Results and discussions

The crystallinity and phase purities of representative BYO and Bi^{3+}, Eu^{3+} doped BYO compounds were identified to assess other samples using X-ray powder diffraction (XRD), which are displayed in Fig. 1. All the XRD patterns involved on the left in Fig. 1 match well with the standard reference of trigonal $Ba_3Y_4O_9$ (JCPDS 38-1377), and no any traces of impurity phases can be observed, indicating single phase BYO phosphors have been acquired, and introductions of Bi^{3+} and Eu^{3+} into this host produce little impurity or induce any significant change to crystal structure. Fig. 2 presents the 3-dimension crystal structure of $Ba_3Y_4O_9$ compound as viewed in a proper direction. We can observe that there are four distinct kinds of Y atoms sites in the structure, all of which are coordinated with six oxygen atoms around to form YO_6 octahedron and locate at 3a sites, while the category of oxygen is different, defined as Y1, Y2, Y3 and Y4. Beside, three different kinds of Ba atoms, named Ba1, Ba2 and Ba3, also can be found in the crystal structure of $Ba_3Y_4O_9$. They also all locate at the wyckoff position of 3a sites with corresponding coordination number of six, six and three, respectively. Selected Y-O bond distances have been listed in Table 1. We can see that the average Y-O distances in different sites are different from each other. Only three kinds of oxygen atoms can be observed and the connections of oxygen atoms with Ba and Y atoms form the

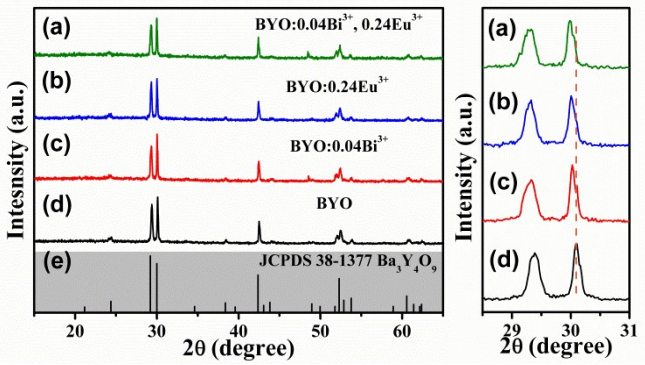

Fig. 1 XRD patterns of $Ba_3Y_4O_9$ host (a) and BYO:0.04Bi^{3+} (b), BYO:0.24Eu^{3+} (c), BYO:0.04Bi^{3+},0.24Eu^{3+} (d), and standard reference card of $Ba_3Y_4O_9$ (JCPDS 38-1377) on the left. Enlarged scale with the corresponding 2θ from 28 to 31 degrees on the right.

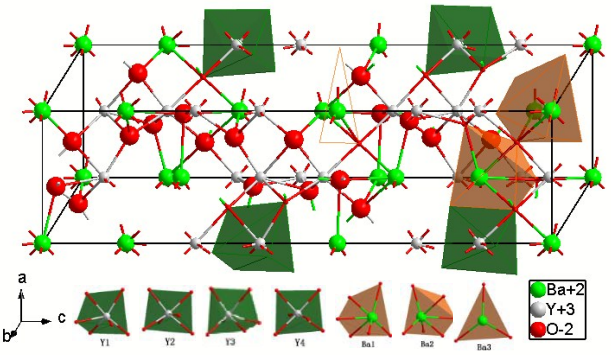

Fig. 2 Crystal structure of $Ba_3Y_4O_9$ host with corresponding trigonal system and different coordination environments of Y and Ba atoms.

structural network. On the basis of the effective ionic radii and charge balance of cations with different coordination numbers, we propose that Bi^{3+} [r = 1.02 Å, coordination number (CN) = 6] and Eu^{3+} (r = 0.95 Å, CN = 6) are preferable to substitute Y^{3+} (r = 0.90 Å) sites, while Ba^{2+} (r = 1.36 Å, CN = 6) is much bigger for them to occupy, as well as the mismatch of valence state. Moreover, the radius percentage difference between the doped ions (Bi^{3+}, Eu^{3+}) and the possible substituted ions Y^{3+} in BYO were calculated and listed in Table 2, based on the formula below:[6]

$$D_r = 100 \times \frac{R_m(CN) - R_d(CN)}{R_m(CN)} \quad (1)$$

Where D_r represents the radius percentage difference; *CN* refers to the coordination number; $R_m(CN)$ and $R_d(CN)$ are the radius of the host cation and the doped ion, respectively. The calculated values are all reasonable (<30%), which indicates it is prior for Bi^{3+} and Eu^{3+} ions to occupy the Y^{3+} sites, consistent with the former discussion results. As mentioned above, the radii of Bi^{3+} and Eu^{3+} ions are bigger than that of Y^{3+}, therefore, the XRD peaks shift to smaller angle when Bi^{3+} and Eu^{3+} were co-doped into BYO host and the shifted extent is proportional to dopant quantity, as depicted on the right in Fig. 1, since the interplanar spacing increases with the introduction of bigger ions on the basis of equation 2dsinθ = nλ,[7] where d is the interplanar spacing, θ is the half diffraction angle, n is the integer, and λ is the fixed wavelength of X-ray.

Table 1 Selected Y-O bond lengths in the BYO compound.

Selected atoms	Bond length	Selected atoms	Bond length	Average bond length
Y1-O2	2.262 Å (three)	Y1-O3	2.434 Å (three)	2.348 Å
Y2-O1	2.277 Å (three)	Y2-O2	2.220 Å (three)	2.2485 Å
Y3-O2	2.490 Å (three)	Y3-O3	2.207 Å (three)	2.3485 Å
Y4-O1	2.214 Å (three)	Y4-O3	2.240 Å (three)	2.227 Å

Table 2 Ionic radii difference percentage (D_r) for a given CN = 6 between matrix cations and doped ions.

Ions	Wyckoff sites	Radius (Å)	Dr
Y^{3+}	3a	0.90	0
Bi^{3+}	3a	1.02	11.7%
Eu^{3+}	3a	0.95	5.3%

The morphologies of representative BYO:0.04Bi^{3+} and BYO:0.04Bi^{3+},0.24Eu^{3+} in Fig. 3 show that some particles are aggregated together to form agglomerate, the size of the particles and agglomerate ranges from about 2 to 12 μm, which is considered to be suitable for encapsulation of LED.

Fig. 4 presents the PL emission and excitation spectra of BYO:0.04Bi^{3+}, BYO:0.24Eu^{3+} and BYO:0.04Bi^{3+},0.24Eu^{3+} phosphors. As depicted in Fig. 4a, we can see that the excitation spectrum monitored at 523 nm extends from 200 nm to 400 nm have two main bumps with the maximum one at 346 nm. Optimal excitation band centered at 346 nm can be accounted for the spin-allowed $^1S_0$-$^3P_1$ transition of Bi^{3+}. As depicted in the previous report, quantitative relationship between A ($^1S_0$-$^3P_1$) and C ($^1S_0$-$^1P_1$) bands can be expressed as:[8]

$$E_C = 3.236 + 2.290\left(E_A - 2.972\right)^{0.865} \quad (2)$$

Where E_C and E_A are the absorption energy of $^1S_0$-$^3P_1$ and $^1S_0$-$^1P_1$ transitions, respectively. Therefore, the value of E_C is calculated to be 4.759 eV (261 nm), Indicating the first bump around at 260 nm is ascribed to the transition of $^1S_0$-$^1P_1$ originating from Bi^{3+} in the excitation spectrum. Under 346 nm excitation, the emission spectrum of BYO:0.04Bi^{3+} presents an asymmetric band with the wavelength range from 350 to 675 nm peaking at 523 nm, corresponding to a greenish yellow-emitting color. As listed in Table 1, there exist four different crystallographic sites with corresponding Y-O bond lengths in BYO crystal structure, producing four kinds of different crystal field strengths. Therefore, the emission band can be approximately decomposed into four symmetric bands with the emission peaks at 385, 417, 487 and 541 nm, which can be assigned to Bi^{3+} substituting Y3, Y1, Y2 and Y4 sites, respectively, because the shorter band length is, the higher covalence of Bi^{3+}-O^{2-} would be caused,[9] resulting in the higher crystal field strength. The variation of emission intensity of Bi^{3+} singly-doped BYO samples is plotted in Fig. 5a. The intensity increases to the maximum until Bi^{3+} concentration x = 0.04, beyond which it begins to descend with further Bi^{3+} content. This phenomenon is attributed to the common concentration quenching effect. It is accepted that energy transfer among Bi^{3+} ions mainly results in the concentration quenching, and the probability of this rises with increasing doped Bi^{3+} concentration until the energy is consumed. In order to analyze the energy transfer mechanism between Bi^{3+} in BYO, the critical distance is needed to be determined by following formula:[10]

$$R_c \approx 2\left[\frac{3V}{4\pi X_c N}\right]^{1/3} \quad (3)$$

where X_c is the critical concentration of dopant ions, N is the number of Z is the number of formula units per unit cell, V refers to the volume of the unit cell. For this host, N = 3, V = 814.40 Å^3, and X_c is 0.04 for Bi^{3+}; Accordingly, the critical distance (R_c) was estimated to be about 23.49 Å. Energy transfer is generally processed via radiation reabsorption, exchange interaction or electric multipolar interactions mechanisms. The radiation reabsorption requests a large overlap of the excitation and emission spectra of the donor and the acceptor, which is little considered to be occurred. And for the exchange interaction, the critical distance is approximately 5 Å, much smaller than that of obtained above. Based on the simple analysis above, it seems that the electric multipolar interactions would be most possible to contribute to the process of energy transfer. According to Dexter and Van Uitert, the expression proposed by them for this can be delivered as:[11]

$$\frac{I}{x} = \left[1 + \beta\left(x\right)^{\theta/3}\right]^{-1} \quad (4)$$

where x and I represent the activator ion concentration and its corresponding emission intensity of certain sample, respectively, and β represents a constant for the given matrix under the same

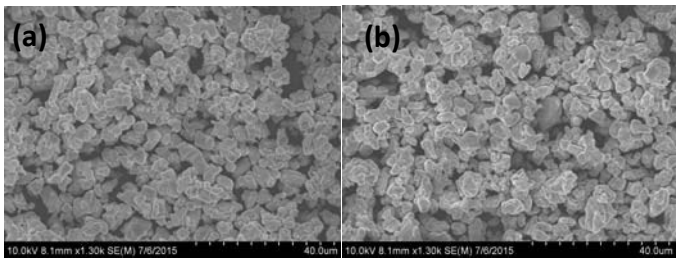

Fig. 3 SEM images of BYO:0.04Bi^{3+} (a) and BYO:0.04Bi^{3+},0.24Eu^{3+} (b) phosphors.

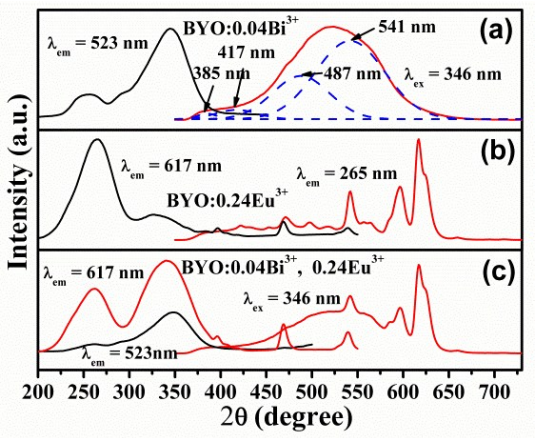

Fig. 4 PL emission and excitation spectra of BYO:0.04Bi^{3+} (a), BYO:0.24Eu^{3+} (c), and BYO:0.04Bi^{3+},0.24Eu^{3+} phosphors.

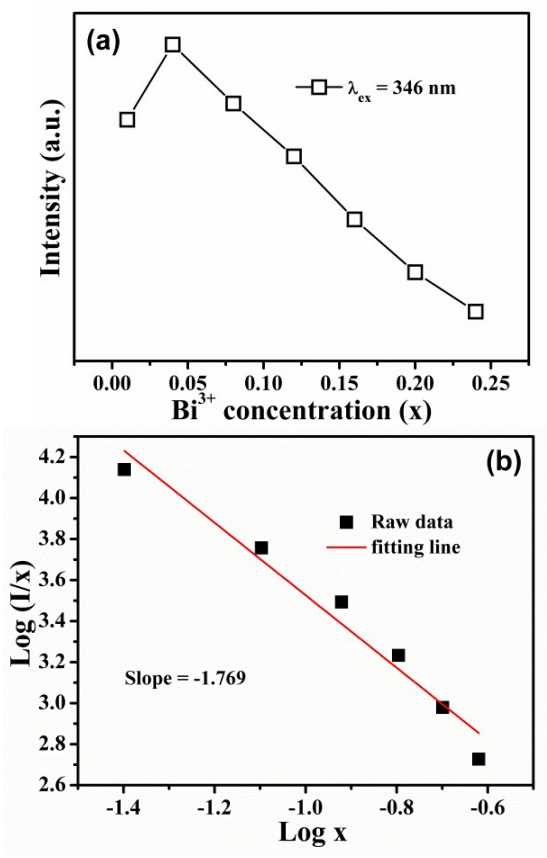

Fig. 5 (a) Variation of Bi^{3+} emission intensity as a function of Bi^{3+} content x in BYO:xBi^{3+} samples. (b) The fitting linear relationship between log (I/x) and log x of Bi^{3+}.

excitation conditions. The energy transfer mechanism of electric multipolar interaction can be approximately determined by analyzing the value of parameter θ from this formula. The values of θ = 6, 8 and 10 correspond to electric dipole-dipole, dipole-quadrupole and quadrupole-quadrupole interactions, respectively. Fig. 5b presents the fitting linear relationship between log(I/xBi^{3+}) and log(xBi^{3+}) with the slope = -θ/3 = -1.769, thus, the θ is determined to be 5.307, close to 6, indicating the dipole-dipole interaction dominates the energy transfer mechanism between Bi^{3+} ions.

The PL excitation spectrum of BYO:0.24Eu^{3+} monitored at 617 nm in Fig. 4b displays two main wide bands from 200 to 375 nm centered at 264 and 326 nm, and many obvious excitation lines at about 384, 396, 468, 539 nm. The former two bands can be attributed to the Eu^{3+}-O^{2-} charge transfer transition and host absorption, and the later excitation lines are originated from the Eu^{3+} transitions of $^5D_0$-$^5L_7$, $^7F_0$-$^5L_6$, $^7F_0$-$^5D_2$, $^7F_0$-$^5D_1$, respectively, as depicted in Fig. 4b. Upon 265 nm excitation, the emission spectrum presents many obvious lines from Eu^{3+} characteristic transition including $^5D_3$-$^7F_1$ (420 nm), $^5D_2$-$^7F_0$ (470 nm), $^5D_2$-$^7F_3$ (498 nm), $^5D_1$-$^7F_0$ (517 nm), $^5D_1$-$^7F_1$ (542 nm), $^5D_1$-$^7F_2$ (563 nm), $^5D_0$-$^7F_1$ (596 nm), $^5D_0$-$^7F_2$ (617 nm) and $^5D_0$-$^7F_3$ (660 nm). The emission at 596 nm derives from $^5D_0$-$^7F_1$ magnetic dipole transition of the Eu^{3+} ions and this transition is insensitive to site symmetry, while the red emission transition $^5D_0$-$^7F_2$ at 617 nm is electric dipole transition aroused by the lack of inversion symmetry at Eu^{3+} sites. As presented in Fig. 4b, the hypersensitive transition $^5D_0$-$^7F_2$ is dominated in its emission spectrum, therefore, we can deduce that the Eu^{3+} ions are located at low local symmetry sites. Considering the valence state and the ionic radius, the doped Eu^{3+} ions occupy the Y^{3+} sites in $Ba_3Y_4O_9$, as discussed above, resulting in the $^5D_0$-$^7F_2$ emission of Eu^{3+} being the prominent peak in the emission spectrum. Compared with the Bi^{3+} emission band and Eu^{3+} excitation lines, an overlap can be observed, therefore, the resonance type energy transfer probability from Bi^{3+} to Eu^{3+} ions can be inferred from it. Fig. 4c depicts the PL emission and excitation spectra of BYO:0.04Bi^{3+},0.24Eu^{3+} sample. Upon 346 nm excitation, the emission spectrum consists of both Bi^{3+} and Eu^{3+} emission bands from 350 to 700 nm, thus, the color tuning from greenish yellow to orange red can be generated by adjusting the mole ratio of Bi^{3+} and Eu^{3+} concentration in BYO:Bi^{3+},Eu^{3+}. Moreover, the excitation spectra monitored at 523 nm (Bi^{3+} emission peak) and 617 nm (Eu^{3+} emission peak) were similar to Bi^{3+} singly-doped BYO sample. This result can be used to certify the existence of energy transfer from Bi^{3+} to Eu^{3+} ions in BYO.

Detailed experiments were performed to adjust the emission color of this series of BYO:0.04Bi^{3+},yEu^{3+} with increasing Eu^{3+} content. Fig. 6a and b show the variations of emission spectra and their corresponding intensities of BYO:0.04Bi^{3+},yEu^{3+} with different Eu^{3+} concentrations under 346 nm excitation, respectively. It can be seen the Bi^{3+} emission intensity decreases monotonously, which is contrary to that of Eu^{3+} in this experimental interval in Fig. 6b. This phenomenon can further demonstrate the energy transfer from Bi^{3+} to Eu^{3+} ions in BYO host. As a result, color tuning from greenish yellow to orange red can be realized in BYO:Bi^{3+},Eu^{3+} system by adjusting the concentration ratio of Bi^{3+} to Eu^{3+}.

Generally, the demonstration of energy transfer from Bi^{3+} to Eu^{3+} ions also can be given by the investigation of the luminescence dynamics. The photoluminescence decay curves of Bi^{3+} under 346 nm excitation and detected at 523 nm in BYO:0.04Bi^{3+},yEu^{3+} were plotted in Fig. 7. As for these as-prepared samples, the decay curves are well fitted with a second-order exponential decay defined as follow:[12]

$$I(t) = I_0 + A_1 \exp\left(\frac{-t}{\tau_1}\right) + A_2 \exp\left(\frac{-t}{\tau_2}\right) \quad (5)$$

where t is the time, $I(t)$ is the corresponding luminescence intensity, A_1 and A_2 are constants, and τ_1 and τ_2 are rapid and slow decay time for the exponential components, respectively. Based on the fitted parameters in equation (5), the value of average lifetime τ^* can be acquired utilizing the formula below:

$$\tau^* = \frac{A_1\tau_1^2 + A_2\tau_2^2}{A_1\tau_1 + A_1\tau_1} \quad (6)$$

Consequently, the decay times of Bi^{3+} emission at 523 nm are determined to be 657.5, 533.4, 432.4, 368.5 and 297.3 ns, corresponding to the Eu^{3+} content y = 0, 0.08, 0.16, 0.24 and 0.32 in BYO:0.04Bi^{3+},yEu^{3+}. It is clear that the evident decrease of decay times occurs with increasing Eu^{3+} concentration, which strongly testifies the energy transfer from Bi^{3+} to Eu^{3+} ions in BYO:0.04Bi^{3+},Eu^{3+} phosphors.

Additionally, the energy transfer efficiency(η_T) from Bi^{3+} to Eu^{3+} ions can be calculated from the variation of emission intensity by using the following equation:[13]

$$\eta_T = 1 - \frac{I_S}{I_{S0}} \quad (7)$$

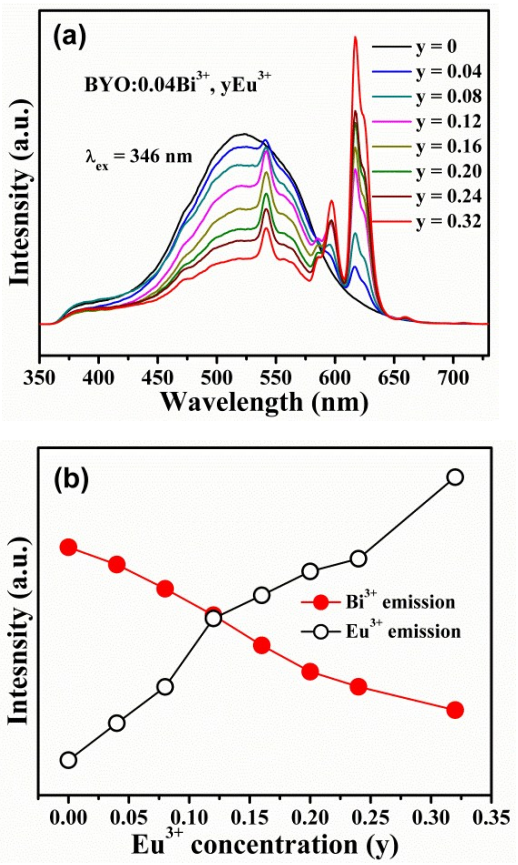

Fig. 6 (a) PL emission spectra of BYO:0.04Bi^{3+},yEu^{3+} phosphors under 346 nm excitation with different concentrations of Eu^{3+}. (b) Dependence of Bi^{3+} and Eu^{3+} emission intensities on Eu^{3+} concentration y.

where η_T is the energy transfer efficiency, I_{S0} and I_S are the corresponding luminescence intensities of Bi^{3+} ions with the absence and presence of Eu^{3+} ions, respectively. Accordingly, the energy transfer from Bi^{3+} to Eu^{3+} increases gradually with increasing Eu^{3+} content in BYO:0.04Bi^{3+},Eu^{3+}, as plotted in Fig. 8. The maximum value is approximately 64% in this interval.

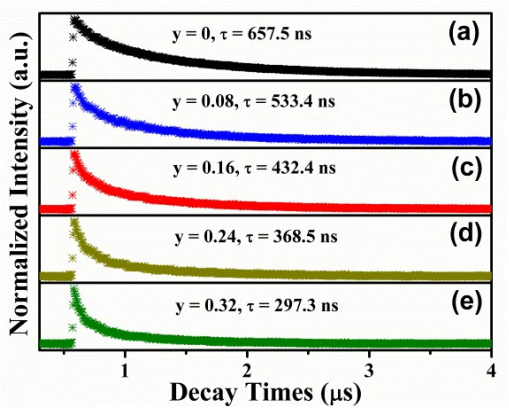

Fig. 7 Fluorescent decay curves of BYO:0.04Bi^{3+},yEu^{3+} (a-e correspond to y = 0-0.32) monitored at 523 nm with the excitation wavelength of 346 nm.

Fig. 9a show the variation of CIE chromaticity coordinates under 346 nm excitation and the digital luminescence photographs under 365 nm UV lamp excitation with corresponding BYO:0.04Bi^{3+},Eu^{3+} samples, respectively. It is well accepted that both emission color tuning and variation of CIE chromaticity coordinates from green area to red area can be obviously observed based on the energy transfer from Bi^{3+} to Eu^{3+} ions in BYO:Bi^{3+},Eu^{3+} system. Detailed CIE coordinate values upon 346 nm excitation are listed in Table 3. It varies from (0.261, 0.459) to (0.575, 0.340) with corresponding Eu^{3+} content y = 0 and 0.32 in BYO:0.04Bi^{3+},yEu^{3+}. Moreover, absolute quantum yield (QY), another important parameter, of as-prepared samples was measured using an integrating sphere, which can be calculated based on the equation below:[14]

$$\eta = \frac{\int L_{emission}}{\int E_{blank} - \int E_{sample}} \quad (8)$$

where $L_{emission}$ represents the integrated area under the emission spectrum, E_{blank} and E_{sample} are the integrated area under the "excitation" band of the blank and the integrated area under the excitation band of the sample (as the sample absorbs part of the light, this value will be much smaller than E_{blank}), respectively. The maximum value is 41.3% for BYO:0.04Bi^{3+},0.24Eu^{3+} sample under 346 nm excitation. Moreover, the absorption values of as-prepared were also measured and listed in Table 3, which are utilized to calculate the external quantum efficiencies. Fig. 9b depicts the simplified energy transfer process from Bi^{3+} to Eu^{3+} ions energy levels. We propose the electrons in ground level of Bi^{3+} $^1S_0$ absorb the excitation energy and then jump to excited state $^3P_1$, some electrons relax to ground state to produce broad band luminescence in greenish yellow region, some of them are transferred to Eu^{3+} $^5D_4$ energy level based on the overlap of emission energy of Bi^{3+} and the excitation energy of Eu^{3+}, and the emission of Bi^{3+} partly quenches. Meanwhile, Eu^{3+} ion can also arises to $^5D_4$ from ground state, and then all the energy fall down to first excited state $^5D_0$. Then, many transitions from Eu^{3+} produce many emission lines.

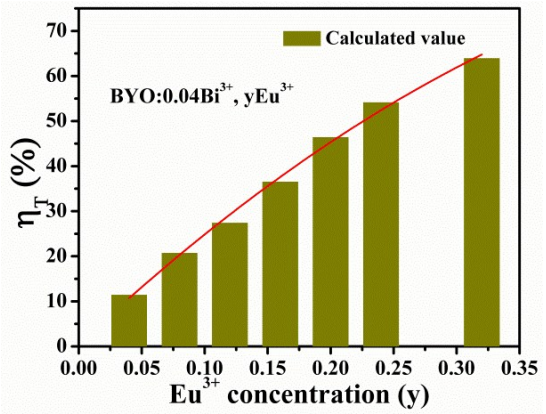

Fig. 8 Energy transfer efficiency (η_T) from Bi^{3+} to Eu^{3+} ions as a function of Eu^{3+} concentration y in BYO:0.04Bi^{3+},yEu^{3+} samples.

Normally, the energy transfer from the sensitizer to the activator processes via a multipolar interaction or an exchange interaction at a higher concentration. On account of Dexter's energy transfer proposal of multipolar interaction, the following formula can be obtained:[15]

$$\frac{\eta_{S0}}{\eta_S} \propto C^{\alpha/3} \quad (9)$$

where η_{S0} and η_S are the luminescence quantum efficiencies of Bi^{3+} ions with the absence and presence of Eu^{3+} ions, respectively. C is the sum of Bi^{3+} and Eu^{3+} contents. α = 6, 8 and 10 correspond to dipole-dipole, dipole-quadrupole, and quadrupole-quadrupole interactions, respectively. Considering that the η_{S0}/η_S is not easy to be determined, we adopted the I_{S0}/I_S as the substitute to assess the discussion, as presented below:

$$\frac{I_{S0}}{I_S} \propto C^{\alpha/3} \quad (10)$$

We can observe that the fitting relationship in Fig. 10b is better than other two in Fig. 10a and c, illustrating dipole-quadrupole interaction dominates the energy transfer process from Bi^{3+} to Eu^{3+} ions in BYO:Bi^{3+},Eu^{3+} samples. The R_c between Bi^{3+} and Eu^{3+} can be calculated to be 12.90 Å using the equation 4, in which the difference is X_c = 0.24 (total concentration of Bi^{3+} and Eu^{3+}), that is, the luminescence intensity of Bi^{3+} is half of that in the sample without Eu^{3+}. Moreover, it also can be obtained through spectral overlap way delivered by following equation:[16]

$$R_c^8 = 3.024\times10^{12}\lambda_S^2 f_q \int f_S(E) f_A(E)/E^4 dE \quad (11)$$

where f_q represents the oscillator strength of the dipole-quadrupole electric absorption transition of the activator, and λ_S (5230 Å) and E stand for the wavelength of strongest intensity of Bi^{3+} and the energy involved in the transfer process(in eV), respectively; $\int f_S(E)f_A(E)/E^4\ dE$ refers to the spectral overlap between the normalized shapes of the sensitizer Bi^{3+} emission $f_S(E)$ and the activator Eu^{3+} excitation $f_A(E)$, and it is determined to be about 0.000995 eV^{-1}. In our case, it is unfortunate that detailed value f_q of Eu^{3+} has not been reported so far. However, Verstegen et al. suggested that f_q/f_d= 10^{-3}-10^{-2} can be reasonable, f_d = 10^{-6} is the oscillator strength for the electric dipole transitions;[17] Accordingly, the value of R_c is determined to be 9.76-13.01 Å, which is in accordance with that calculated by concentration quenching method above (12.90 Å). This result can further give us a confirmation that the electric dipole-quadrupole interaction can be responsible for the energy transfer mechanism from Bi^{3+} to Eu^{3+} ions in BYO:Bi^{3+},Eu^{3+} samples.

PL thermal property is one of the important parameters for phosphors applied in LEDs. Herein, we obtained the temperature-dependent PL emission spectra with the temperature range from 25 to 200 ℃ to assess the influence of temperature on luminescence and determine the activation energy for thermal quenching, as depicted in Fig. 11. We can find the emission intensity of Bi^{3+} and Eu^{3+} in BYO:0.04Bi^{3+},0.24Eu^{3+} descend monotonously with increasing measured temperature, while the declined rates are

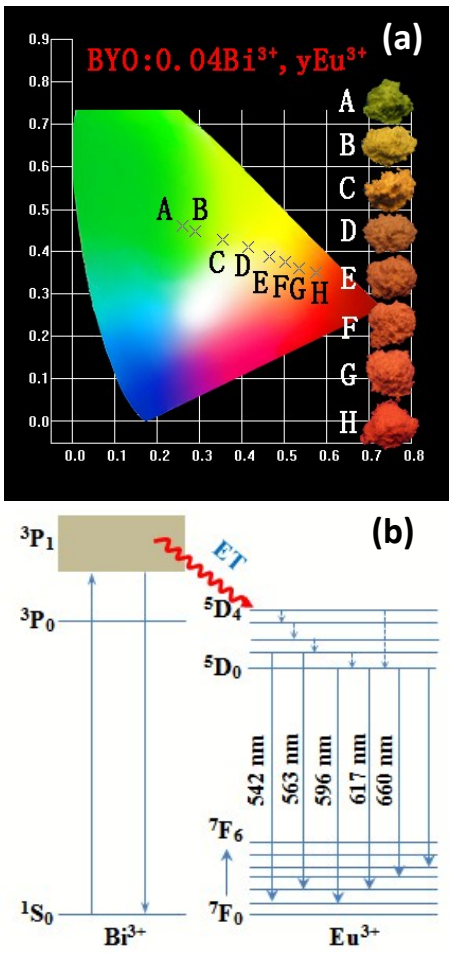

Fig. 9 (a) Variation of CIE chromatic coordinate as a function of Eu^{3+} concentration y in BYO:0.04Bi^{3+},yEu^{3+} samples under 346 nm excitation (Inset is the luminescent photos under 365 nm UV lamp excitation). (b) Simple scheme of energy transfer (ET) from Bi^{3+} to Eu^{3+} ions.

different because the energy transfer effect is also influenced by temperature. The reason for the decrease of emission intensity is generally ascribed to the thermal quenching via the thermal activation through the crossing point between the ground and the excited states. The emission intensities of Bi^{3+} and Eu^{3+} at 150 ℃ retain about 51% and 37% of their corresponding initial values at room temperature, respectively. The Arrhenius formula below is utilized to assess the activation energy:[18]

$$In\left(\frac{I_0}{I}\right) = InA - \frac{E_a}{kT} \quad (12)$$

where E_a and T represent the objective activation energy and temperature (K). A is a constant, and k is the Boltzmann constant (8.626×10^{-5} eV). I_0 and I correspond to the integrated intensity at the room and differently operated temperatures, respectively. Therefore, the relationship of $In(I_0/I-1)$ versus 1/kT activation energy graph for thermal quenching of BYO:0.04Bi^{3+},0.24Eu^{3+} phosphor was plotted in Fig. 11b, which shows the slope of fitting line is -0.2055, thus the activation energy E_a can be approximately 0.2055 eV. The relative high value indicates its good thermal properties.

Table 3 Calculated CIE chromatic coordinates of BYO:0.04Bi^{3+},yEu^{3+} samples and their corresponding QYs and absorption values under 346 nm excitation.

Sample No.	Eu^{3+} concentration (y mol)	CIE coordinates (x, y)	QY(%)/ Absorption(%)
A	0	(0.261, 0.459)	24.7/22.9
B	0.04	(0.291, 0.447)	31.8/28.7
C	0.08	(0.354, 0.427)	33.4/27.5
D	0.12	(0.415, 0.410)	35.7/30.1
E	0.16	(0.466, 0.387)	31.2/32.7
F	0.20	(0.503, 0.374)	40.2/28.3
G	0.24	(0.535, 0.359)	41.3/26.8
H	0.32	(0.575, 0.340)	40.8/27.3

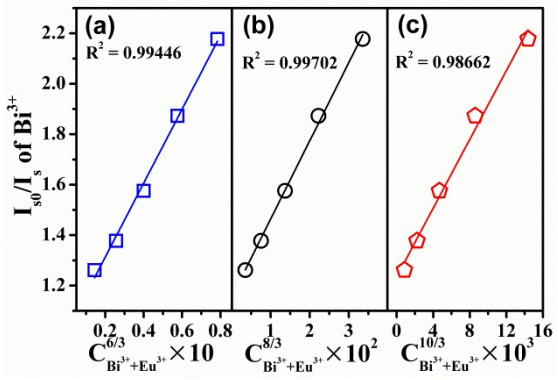

Fig. 10 Dependence of (I_{S0}/I_S) of Bi^{3+} on (a) $C^{6/3}$ (b) $C^{8/3}$ and (c) $C^{10/3}$ in BYO:Bi^{3+},Eu^{3+} samples.

4. Conclusions

A series of novel $Ba_3Y_4O_9$:Bi^{3+},Eu^{3+} phosphors were first synthesized via the high-temperature solid state reaction process. Bi^{3+} singly-doped BYO sample presents intense greenish-yellow color under UV excitation with the emission wavelength range of 350-675 nm centered at 523 nm. When Eu^{3+} were co-doped into $Ba_3Y_4O_9$:Bi^{3+}, the tunable color from greenish yellow to orange red occurs by simply adjusting the Eu^{3+} content, which is based on the energy transfer from Bi^{3+} to Eu^{3+} ions in $Ba_3Y_4O_9$:Bi^{3+},Eu^{3+}. The energy transfer possibility is inferred from the overlap of Bi^{3+} emission and Eu^{3+} excitation spectra, and then demonstrated by the variation of emission and decay times of Bi^{3+} in Bi^{3+}, Eu^{3+} co-doped $Ba_3Y_4O_9$ phosphors. Moreover, the energy transfer mechanism from Bi^{3+} to Eu^{3+} ions in BYO host is determined to be a resonant type via electric dipole-quadrupole interaction, which is also validated by the consistence of critical distance between Bi^{3+} and Eu^{3+} ions calculated by concentration quenching (12.90 Å) and spectral overlap (9.76-13.01 Å) methods. These results indicate that $Ba_3Y_4O_9$:Bi^{3+},Eu^{3+} may serve as a potential color-tunable phosphor for UV-pumped LED devices.

Acknowledgments

This project is financially supported by the Scientific and Technological Department of Jilin Province (Grant No. 20150520029JH), National Natural Science Foundation of China (NSFC Grants 51472234, 51172227, 91433110), National Basic Research Program of China (Grants 2014CB643803), and Joint Funds of the National Natural Science Foundation of China (Grant U13012038).

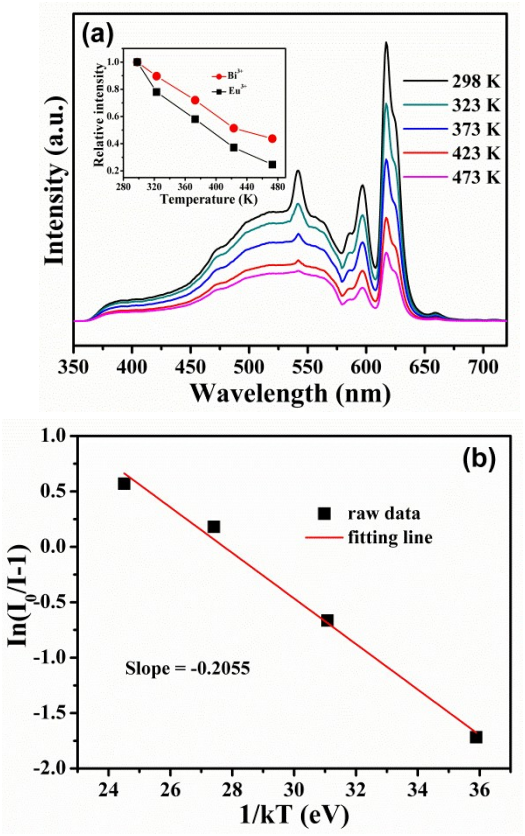

Fig. 11 (a) Dependence of emission spectra of BYO:0.04Bi^{3+},0.24Eu^{3+} on temperature, inset is the variations of emission intensity of Bi^{3+} and Eu^{3+}. (b) Linear relationship of $\ln(I_0/I-1)$ versus 1/kT activation energy graph for thermal quenching for BYO:0.04Bi^{3+},0.24Eu^{3+} sample.

References

1 (a) E. F. Schubert and J. K. Kim, *Science*, 2005, **308**, 1274; (b) K. A. Denault, J. Brgoch, M. W. Gaultois, A. Mikhailovsky, R. Petry, H. Winkler, S. P. DenBaars and R. Seshadri, *Chem. Mater.*, 2014, **26**, 2275; (c) L. Chen, C.-C. Lin, C.-W. Yeh and R.-S. Liu, *Materials*, 2010, **3**, 2172.

2 (a) H. S. Jang, W. B. Im, D. C. Lee, D. Y. Jeon and S. S. Kim, *J. Lumin.*, 2007, **126**, 371; (b) G. S. R. Raju, E. Pavitra, G. Nagaraju and J. S. Yu, *Dalton Trans.*, 2015, **44**, 1790.

3 (a) F. Kang, M. Peng, Q. Zhang and J. Qiu, *Chem. Eur. J.*, 2014, **20**, 11522; (b) Z. Yang, Z. Zhao, Y. Wen and Y. Wang, *J. Alloys Compd.*, 2013, **559**, 142. (c) C. Liu, Z. Xia, M. S. Molokeev and Q. Liu, *J. Am. Ceram. Soc.*, 2015, **98**, 187.

4 (a) H. Zhu, Z. Xia, H. Liu, R. Mi and Z. Hui, *Mater. Res. Bull.*, 2013, **48**, 3513; (b) F. Kang, M. Peng, X. Yang, G. Dong, G. Nie, W. Liang, S. Xu and J. Qiu, *J. Mater. Chem. C*, 2014, **2**, 6068; (c) S. Zhang, Y. Hu, R. Chen, X. Wang and Z. Wang, *Opt. Mater.*, 2014, **36**, 1830; (d) H. Ju, J. Liu, B. Wang, X. Tao, Y. Ma and S. Xu, *Ceram. Inter.*, 2013, **39**, 857; (e) F. Kang, Y. Zhang and M. Peng, *Inorg. Chem.*,

2015, **54**, 1462; (f) T. Matsunaga, S. Takeshita and T. Isobe, *J. Lumin*., 2015, **165**, 62; (g) S. Yan, J. Zhang, X. Zhang, S. Lu, X. Ren, Z. Nie and X. Wang, *J. Phys. Chem. C*, 2007, **111**, 13256; (h) P. Du, L. K. Bharat and J. S. Yu, *J. Alloys Compd*., 2015, **633**, 37; (i) F. Kang, Y. Zhang, L. Wondraczek, J. Zhu, X. Yang and M. Peng, *J. Mater. Chem. C*, 2014, **2**, 9850.

5 C. R. Ronda, *J. Lumin*. 1997, **72**, 49.

6 (a) H. Liu, Y. Luo, Z. Mao, L. Liao and Z. Xia, *J. Mater. Chem. C*, 2014, **2**, 1619; (b) W. Lv, W. Lu, N. Guo, Y. Jia, Q. Zhao, M. Jiao, B. Shao and H. You, *RSC Advances*, 2013, **3**, 16034.

7 C. R. Volker Bachmann, O. Oeckler, W. Schnick and A. Meijerink, Chem. Mater., 2009, **21**, 316.

8 L. Wang, Q. Sun, Q. Liu and J. Shi, *J. Solid State Chem*., 2012, **191**, 142.

9 H. Ju, W. Deng, B. Wang, J. Liu, X. Tao and S. Xu, *J. Alloys Compd*., 2012, **516**,153.

10 (a) G. Blasse, *J. Solid State Chem*., 1986, **62**, 207; (b) S.-P. Lee, C.-H. Huang and T.-M. Chen, *J. Mater. Chem. C*, 2014, **2**, 8925.

11 (a) L. G. Van Uitert, *J. Electrochem. Soc*., 1967, **114**, 1048; (b) A. Watras, P. J. Deren' and R. Pazik, *New J. Chem*., 2014, **38**, 5058.

12 (a) M. P. Saradhi and U. V. Varadaraju, Chem. Mater., 2006, **18**, 5267; (b) P. Li, Z. Wang, Z. Yang and Q. Guo, *J. Mater. Chem. C*, 2014, **2**, 7823.

13 (a) P. I. Paulose, G. Jose, V. Thomas, N. V. Unnikrishnan and M. K. R. Warrier, *J. Phys. Chem. Solids*, 2003, **64**, 841; (b) H. Guan, G. Liu, J. Wang, X. Dong and W. Yu, *New J. Chem*., 2014, **38**, 4901.

14 R. V. Deun, D. Ndagsi, J. Liu, I. V. Driessche, K. V. Hecke and A. M. Kaczmarek, *Dalton Trans*., 2015, **44**, 15022.

15 (a) D. L. Dexter, *J. Chem. Phys*., 1953, **21**, 836. (b) J. Chen, Y. Liu, M. Fang, and Z. Huang, *Inorg. Chem*., 2014, **53**, 11396.

16 (a) D. L. Dexter and J. H. Schulman, *J. Chem. Phys*., 1954, **22**, 1063. (b)Y. H. Won, H. S. Jang, W. B. Im, J. S. Lee and D. Y. Jeon, *Appl. Phys. Lett*., 2006, **89**, 231909.

17 J. M. P. J. Verstegen, J. L. Sommerdijk and J. G. Verriet, *J. Lumin*., 1973, **6**, 425.

18 X. Zhang, J. Wang, L. Huang, F. Pan, Y. Chen, B. Lei, M. Peng and M. Wu, *ACS Appl. Mater. Interfaces*, 2015, **7**, 10044.

Graphic Abstract

A series of novel color-tunable $Ba_3Y_4O_9:Bi^{3+}$, Eu^{3+} phosphors have been prepared via the high-temperature solid-state reaction route and investigated.